Experiments in Fluids 29 (2000) 509–518 © Springer-Verlag 2000

Measurement of surfactant properties using a circular capillary wave field

J. R. Saylor, A. J. Szeri, G. P. Foulks

Abstract Measurements of the decay coefficient are presented for three different surfactants as a function of surface concentration. These measurements were obtained using a circular field of capillary waves. Data was purposely obtained close to the center of the tank, where the wave amplitude is large, and meniscus effects are expected to be small. The theory for linear, standing waves in a circular geometry is developed, without the usual assumption $|kr| \gg 1$. The surfactants investigated were: stearic acid, oleyl alcohol and hemicyanine. Measurements of the decay coefficient for hemicyanine have not been obtained heretofore. Several intrinsic benefits of the circular geometry are noted. The potential for improved accuracy in the measurement of surfactant properties using this geometry is suggested.

1 Introduction

It is well known that surfactant monolayers affect the propagation characteristics of waves. The presence of a surfactant monolayer alters the elasticity E and surface tension σ at a gas–liquid interface, thereby changing the measured wavelength λ, and decay coefficient α of the wave field. The restoring force for a capillary wave is surface tension, and hence α and λ are especially sensitive to the concentration and type of surfactant monolayer which is present at the interface for these waves. This fact has made capillary waves an especially useful tool for characterizing surfactant monolayers.

The typical experimental configuration utilized in measuring α and λ is illustrated in Fig. 1. A wave generator and a sensor, which also acts as a wave reflector, are located at opposite ends of a rectangular trough. Typically the generator is a horizontal bar which vibrates in the vertical direction. The reflecting bar is connected to a motion sensitive device, such as a piezoelectric crystal, enabling it to simultaneously reflect the wave and sense its amplitude. The superposition of the generated wave and the reflected wave results in a standing wave field between the generator and reflector. By scanning the reflecting bar over one or more wavelengths, the wavelength and decay coefficient can be obtained.

The method described above was pioneered by Mann and Hansen (1963), and the experimental apparatus and theoretical underpinnings were further developed by several investigators (e.g., Lucassen and Hansen 1966; Bendure and Hansen 1967; Hansen et al. 1968; Mann and Ahmad 1969). Improvements have also been implemented which provide non-contact methods for wave generation (e.g., Sohl et al. 1978) as well as non-contact methods of amplitude measurement (e.g., Garrett and Zisman 1970). A review of the theory and experimental techniques used in obtaining α and λ in a capillary wave field can be found in Hansen and Ahmad (1971).

The aforementioned improvements on the original technique of Mann and Hansen (1963) notwithstanding, the general idea of using a field of capillary waves in a rectangular geometry to characterize a surfactant monolayer has remained essentially the same. Indeed, experiments conducted on many different surfactants over a range of wavelengths and surface concentrations have been performed using this method, and they represent a significant part of the literature on monolayers and capillary waves. There are, however, several drawbacks associated with the rectangular configuration illustrated in Fig. 1, and these are now discussed.

Part of the importance of obtaining α and λ is that these variables, combined with the surface tension, can be related to the elasticity E, a more general measure of the characteristics of a surfactant monolayer. The theory used to relate these variables is linearized and hence it is necessary to perform measurements on wave fields where the amplitude to wavelength ratio is small $(a/\lambda \sim O(10^{-3}))$. Since millimeter-scale capillary waves are typically used in these experiments, micron-scale wave height measure-

Received: 15 April 1999/Accepted: 12 December 1999

J. R. Saylor[1]
Naval Research Laboratory, Washington, DC 20375, USA

A. J. Szeri
University of California, Berkeley, CA 94720, USA

G. P. Foulks
Langley High School, McLean, VA 22101, USA

Present address:
[1] Clemson University, Dept of Mechanical Engineering
Clemson, SC29634-0921, USA

Correspondence to: J. R. Saylor

Financial support from the Office of Naval Research, through the Naval Research Laboratory, as well as the DOD Science and Engineering Apprentice Program is gratefully acknowledged. The authors' gratitude goes also to G.M. Korenowski and J.S. Kelley for construction of the tank and for donation of the hemicyanine which was used in these experiments.

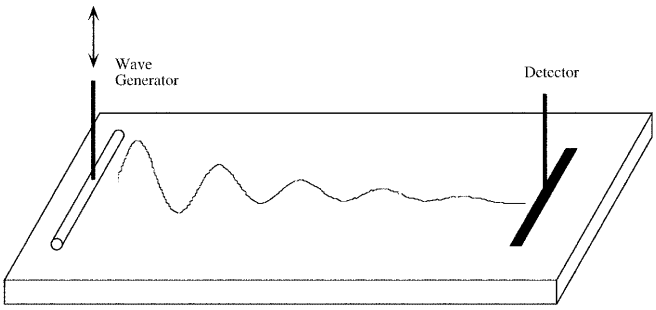

Fig. 1. Standard method used for measuring α and λ. A field of standing capillary waves is generated by creating a planar propagating wave which is then reflected by a sensor

ments are necessary. At such small amplitudes, it is desirable to obtain measurements at regions where the wave height is near its largest, to maximize the signal-to-noise ratio. For the configuration illustrated in Fig. 1, the peak wave height coincides with the location of the wave generator, which is where meniscus and subsurface flow disturbances are largest. Hence, there is an inherent trade-off: one would like to obtain measurements far from the generator, so that meniscus effects are minimized, yet one cannot venture too far from the generator, since the rapidly decaying wave height will quickly be lost in the noise of the measurement system. For situations similar to those illustrated in Fig. 1, the deformation of the free surface due to the meniscus extends a distance proportional to $e^{-x/L}$ where L is the radius of the horizontal member of the wave generator (Allain and Cloitre 1988). The radii of such cross members are typically on the order of 1 mm (preventing deformation of the cross member at smaller diameters is difficult), requiring a distance on the order of 5 mm to reduce the meniscus depression to a level of less than, say, 1%. In typical configurations, the distance between the wave generator and the probe is approximately 1 cm (e.g., Mann and Hansen 1963). Typical damping coefficients are on the order of $\alpha \sim 0.1$ to 1.0 cm^{-1}. Since the wave amplitude decays as $e^{-\alpha x}$ for the rectangular configuration illustrated in Fig. 1, the amplitude decrease from the wave generator to the sensing probe is typically 10–60% or so. Consequently, a comparable increase in the signal-to-noise ratio would be obtained by obtaining measurements where the wave amplitude is largest, assuming a constant level of system noise.

A second drawback of the configuration illustrated in Fig. 1 is that the initially parallel wave fronts acquire three-dimensional characteristics as they propagate from the wave generator. The presence of the side-walls in the trough, or the stagnant liquid at the edge of the propagating wave fronts cause the initially planar wave fronts to acquire curvature, resulting in an error in the amplitude measurement at the detector location. A final drawback is that, in addition to the meniscus which exists at the wave generator, there is also a meniscus at the reflector which can adversely affect measurement reproducibility due to the inherent difficulties associated with contact lines.

All the problems listed above can be reduced or eliminated by performing measurements of α in a circular geometry. An example of a system capable of performing such a measurement is illustrated in Fig. 2. In this configuration, waves are generated by vibrating a circular tank in the vertical direction. This vibration disturbs the meniscus at the tank edge, causing waves to propagate inward in a circular pattern. These waves converge at the center of the tank and reflect back outward. Superposition of these inward traveling and outward traveling waves creates a circular, nearly standing wave field. As illustrated in the figure, measurements of the wave height are performed at, or near, the tank center. These measurements are optical, in the figure, for reasons which will be described below.

Measuring α in a circular wave facility such as that illustrated in Fig. 2 has several advantages over a rectangular setup. In a circular geometry, the peak wave amplitude is located at the geometric center of the tank. This location is also the point which is farthest from the tank rim. Hence, by obtaining wave amplitude measurements at or near the tank center, any adverse effects due to disturbances at the wave generator are minimized, without having to move to a location where the wave height is small. Therefore, the inherent tradeoff which exists in the rectangular geometry is avoided. Furthermore, there is no solid wall which acts as a reflector in this facility; the waves simply reflect from themselves as they converge at the geometric center of the tank. As a result, the wave height detector does not need to also serve as a reflector, and a non-intrusive optical detector can be employed. Thus, the error associated with the meniscus which would be present at the reflector in the rectangular configuration, is avoided in the circular setup. Finally, because there is no 'edge' to a circular wave, there is no deformation of the wave fronts, as they propagate. That is, the problem associated with an alteration of the wave fronts which exists in the rectangular method does not exist in the circular geometry.

In spite of the advantages associated with the circular geometry, few studies have been conducted using this configuration. Thiessen and Scheludko (1967) and Thiessen and Schwartz (1967) both used an apparatus very similar to that illustrated in Fig. 2. However, in their work,

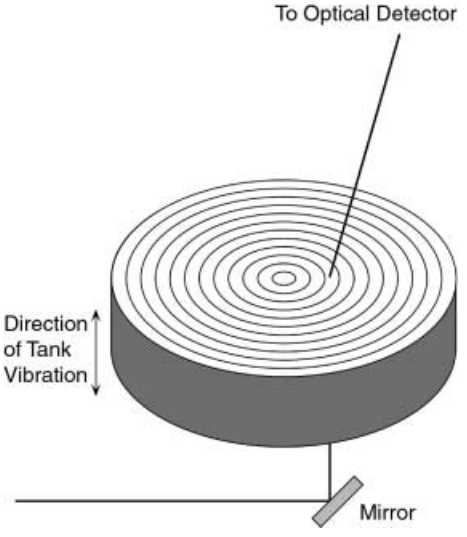

Fig. 2. Set-up for measuring α and λ using a circular field of standing capillary waves. The generator is the tank rim, and measurements of the wave amplitude are obtained near the tank center

measurements were obtained at a large value of $|kr|$, where k is the wavenumber $k = 2\pi/\lambda$, and r is the radial distance from the center of the tank. This choice was apparently made to take advantage of a simplification in the theory describing capillary waves, as will be described in Sect. 2, below. Jiang et al. (1992) investigated circular capillary waves using a slightly different wave generation mechanism than that illustrated in Fig. 2. Instead of generating waves by vibrations at the tank rim, waves were generated at a point by applying a sinusoidal voltage to a needle located close to the water surface. Capillary waves were generated by electrocapillary deflection of the air–water interface, and these waves propagated outward from the location of the needle. Measurements of the wave amplitude were made at different radial locations, and resort to the $|kr| \gg 1$ assumption was again made, requiring measurements at large distances from the tank center.

In the work presented here, capillary waves are generated by providing a vertical vibration to a circular tank. A circular wave field is established, and measurements of the wave amplitude are made at several radial locations, allowing computation of α. In the theory which is developed in Sect. 2, resort to the $|kr| \gg 1$ assumption is avoided allowing for measurements close to the tank center.

Three surfactants were investigated in the experiments described in Sect. 3. Two of these, oleyl alcohol and stearic acid, were chosen because they are commonly studied in the surfactant literature. The third, hemicyanine, has not been as frequently investigated, but recently has been explored because it has a strong non-linear optical response, permitting non-intrusive measurements of surface concentration using second harmonic generation (SHG) (Hirsa et al. 1997a, b). It is anticipated that a combination of the non-invasive technique described here for measuring such surfactant properties as α, and the non-invasive SHG method for measuring surface concentration will provide a powerful method for evaluating surfactant–wave interactions.

2 Theory

The theory for rectilinear capillary waves is nicely presented in Edwards et al. (1991). Work on cylindrical capillary waves, at points distant from the focus, was carried out by Thiessen and Scheludko (1967), Thiessen and Schwartz (1967) and Jiang et al. (1992). In what follows, we present a theory for cylindrical capillary waves without this restriction to points distant from the focus. In the experiments which are described in Sect. 3, the envelope of the wave slope of the standing wave field is measured as a function of radius, over a distance of roughly one and a half wavelengths. The theory developed for cylindrical capillary waves is then applied to this data, and values of the decay coefficient and wavelength are extracted.

2.1 Solutions for traveling waves

A solution for the velocity field of an outward-traveling wave is

$$v_r = -H_1^{(1)}(kr)\mathrm{e}^{i\omega t}(ikA\mathrm{e}^{kz} + mB\mathrm{e}^{mz}) \ , \tag{1}$$

$$v_z = H_0^{(1)}(kr)\mathrm{e}^{i\omega t}(ikA\mathrm{e}^{kz} + kB\mathrm{e}^{mz}) \ . \tag{2}$$

Here r is the radial coordinate, z is elevation, $k = 2\pi/\lambda + i\alpha$ is the complex wavenumber, $H_n^{(i)}$, is the nth order Hankel function of the ith kind, $\omega = 2\pi\nu$ is the radian frequency of the forcing, $m^2 = k^2 + i\omega/\eta$ where η is the kinematic viscosity, and A and B are the amplitudes of the predominantly transverse and predominantly longitudinal components of the wave, respectively. The wave is outward-traveling when $\nu < 0$ and $\alpha > 0$.

The velocity field satisfies the linearized axisymmetric Navier–Stokes equations, along with the associated pressure field. In order to show this, one must make heavy use of the well-known recursion relations for Hankel functions. It is not necessary to pass to the limit $|kr| \gg 1$ and substitute the Hankel functions by their well known asymptotic forms (decaying exponentials). By integrating the velocity field, one obtains the surface elevation

$$\zeta = \zeta_0 H_0^{(1)}(kr)\mathrm{e}^{i\omega t} \ , \tag{3}$$

where ζ_0 is a combination of the amplitudes and other preceding variables.

If, instead of $H_n^{(1)}$ one uses $H_n^{(2)}$ in Eqs. (1) and (2), then one obtains the velocity field of an inward-traveling wave when $\nu < 0$ and $\alpha > 0$. In this case, the surface elevation is simply

$$\zeta = \zeta_0 H_0^{(2)}(kr)\mathrm{e}^{i\omega t} \ . \tag{4}$$

2.2 Dispersion relation

The waves must satisfy the normal and shear stress boundary conditions at the surface ζ. In a linear context, these read as follows. For the normal stress, we require

$$\frac{\sigma}{r}\frac{\partial}{\partial r}\left[r\frac{\partial\zeta}{\partial r}\right] = -p + 2\rho\eta\frac{\partial v_z}{\partial z} \ . \tag{5}$$

Here σ is the surface tension and ρ is the density of the water. The shear stress boundary condition is

$$E^*\frac{\partial}{\partial r}\left[\frac{1}{r}\frac{\partial(r\xi)}{\partial r}\right] = \rho\eta\left[\frac{\partial v_r}{\partial z} + \frac{\partial v_z}{\partial r}\right] \ , \tag{6}$$

where ξ is the surface-parallel displacement, and E^* is the surface elasticity. We note there are several errors in the boundary conditions considered by Jiang et al. (1992), but these appear not to have any consequence in the limit $|kr| \gg 1$ those authors consider.

If we substitute in the expressions for the velocity, pressure and surface elevation fields, and make use once again of the recursion relations among Hankel functions of different order, we obtain

$$A(g\,k\,\rho + k^3\sigma + 2\,i\,k^2\eta\,\rho\,\omega - \rho\,\omega^2) - i\,B\,k(g\,\rho + k^2\sigma + 2\,i\,m\,\eta\,\rho\,\omega) = 0 \ , \tag{7}$$

and

$$A\,k^2(-(E^*\,k) + 2\,i\,\eta\,\rho\,\omega) + B(i\,E^*\,k^2 m + (k^2 + m^2)\eta\,\rho\,\omega) = 0 \ . \tag{8}$$

These are the same expressions found in the study of rectilinear capillary waves (see, e.g., Edwards et al. (1991)). Therefore the dispersion relation found from the solvability condition for the system Eqs. (7) and (8) is also the same.

2.3
Superposition of waves

Our interest in the present work is with a capillary wave produced at the outer edge of a circular domain, which travels inward, is damped, and reflects at the axis of symmetry into an outward-traveling (also damped) wave. The superposition of an inward-traveling wave and an outward traveling wave will feature a cusp in the surface at $r = 0$, unless the amplitudes of the two waves are identical. In this latter case, we have the elevation of the surface.

$$\zeta = \frac{\zeta_0}{2}[H_0^{(1)}(kr) + H_0^{(2)}(kr)]\mathrm{e}^{i\omega t} \quad , \tag{9}$$

which simplifies to (Thiessen and Scheludko 1967; Thiessen and Schwartz 1967)

$$\zeta = \zeta_0 J_0(kr)\mathrm{e}^{i\omega t} \quad . \tag{10}$$

The wave is truly only a standing wave at $r = 0$, where the spatially dependent amplitudes of the inward and outward traveling waves exactly match. For $r > 0$, the outward-traveling wave is strongly damped – hence the composite wave looks more and more like just the inward-traveling wave as one looks at larger and larger r.

2.4
Determination of the complex wavenumber

In the experiments presented here, we measure the envelope of the absolute value of the wave slope as a function of radius along a line, roughly, 0.5 cm in length. This corresponds to the fourth, fifth and sixth extrema in wave slope. So as to avoid having to determine the amplitudes of the waves, it is convenient to use the relative decay of the waves to determine the complex wavenumber.

The slope of the composite wave is the real part of

$$\zeta'(r,t) = -\zeta_0\, k\, J_1(kr)\, \mathrm{e}^{i\omega t} \quad . \tag{11}$$

Following Thiessen and Schwartz (1967), we write

$$\zeta'(r,t) = |\zeta_0||k||J_1(kr)| \exp[i(\omega t + \pi + \arg[\zeta_0] + \arg[k] + \arg[J_1(kr)])] \quad . \tag{12}$$

In the experimental technique we have developed, what is actually measured is the wave slope envelope corresponding to the theoretical envelope $|\zeta_0||k||J_1(kr)|$. To analyze the experimental data, we simply determine the parameters $\{|\zeta_0|, \lambda, \alpha\}$ which lead to the closest match between the theoretical and experimental envelopes over that portion of the experimental envelope which is measured in a given experiment. This procedure is robust and leads to very close agreement between theoretical and experimental envelopes, as we show below. Two final details that should be mentioned in our implementation of this approach are as follows. Because the wave slope envelopes were measured starting from approximately the fourth maximum, and because the radial location of this maximum was not recorded, the data must be shifted by an amount to be determined during the course of the data analysis. Hence we actually determined four parameters rather than the three to which we earlier made reference. Finally, the data analysis was performed using the nonlinear fitting facility in Mathematica, which minimizes the error between the experimental and theoretical wave slope envelopes by searching for a minimum in an error norm over the choice of the four parameters.

2.5
Determination of the surface tension and surface elasticity

Of course, using the (complex) dispersion relation derived for cylindrical capillary waves, it is possible to solve for E^* and σ once λ and α have been extracted from the experimental data. Because the dispersion relationship for cylindrical capillary waves is identical to that for plane capillary waves (Sect. 2.2), the procedure to be followed to determine E^* and σ is the same as that outlined in Lucassen and Hansen (1966) and is not presented here.

3
Experimental method

The experiments were conducted in a small circular glass tank, 22.2 mm high with an internal diameter of 69.8 mm. The rim of the tank was ground flat and coated with a thin film of paraffin. The experimental setup is illustrated in Fig. 3, which shows the side and top views of the apparatus. The glass tank was affixed to an electrodynamic shaker which provided a vertical vibration. Excitation of the tank disturbed the meniscus at the tank edge, creating an inward traveling wave, which was subsequently reflected outward, creating the nominally standing wave field described in Sect. 2. When the water surface was viewed from the appropriate angle, a pattern of concentric circles was readily visible in the reflected image of the ceiling lights. The shaker was driven at 120 Hz, by an amplified sine wave, generated by a precision frequency synthesizer. It is noted that the amplitude of vibration from the electrodynamic shaker was never high enough to exceed the threshold at which Faraday waves formed (Faraday 1831), hence the wave frequency was always equivalent to that of the shaker.

3.1
Wave slope measurement

In order to obtain the surfactant properties using the theory outlined in Sect. 2, a measurement of the envelope of the wave slope along a portion of the tank radius was required. These slope measurements were obtained using a laser slope gauge which is described below. A more detailed description can be found in Saylor and Handler (1997).

A HeNe laser was mounted on an optical table which was physically separate from the table supporting the electrodynamic shaker, insuring that any vibration transmitted through the shaker base was not transmitted to the laser or associated optics. As indicated in Fig. 3a, the beam of the HeNe laser was directed up through the transparent

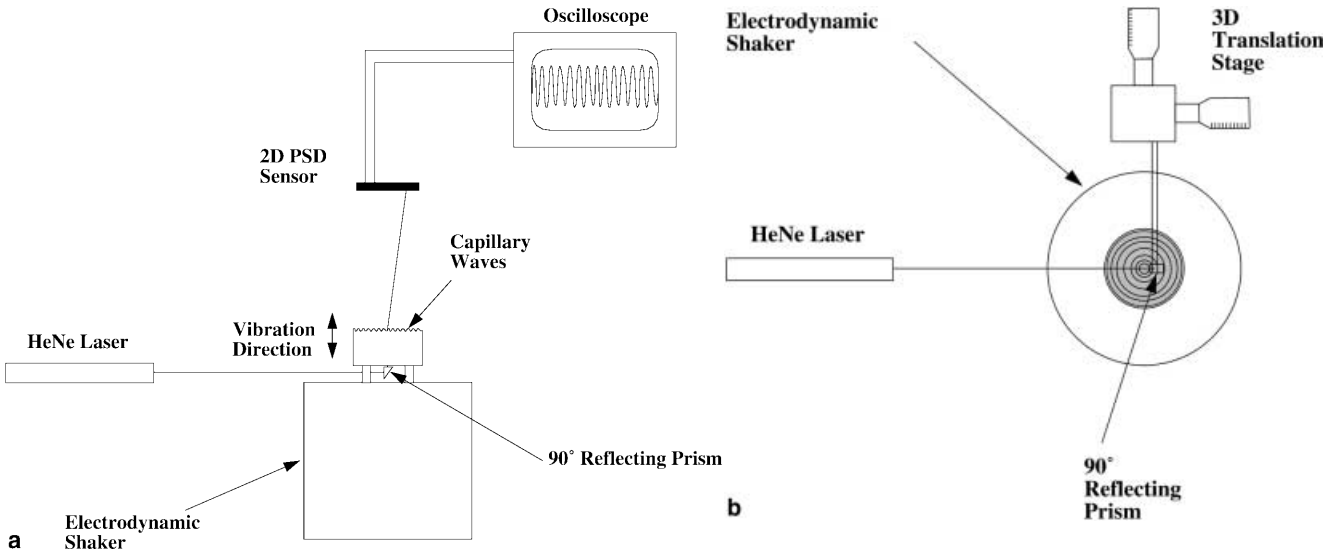

Fig. 3a, b. Illustration of the experimental apparatus: **a** side view, **b** top view. The optics used to focus the HeNe laser beam are omitted and presented in Fig. 4

floor of the tank, using a 90° prism. This prism was mounted on a rotational stage which was adjusted prior to initiation of the experiments insuring that the beam orientation was vertically true.

The laser beam was focused so that the diameter at the air–water interface was sufficiently small to resolve the waves. The focusing optics which lie between the laser and the 90° prism were omitted from Fig. 3 for simplicity, and are presented in Fig. 4. The position of all four lenses was adjusted so that the beam was normal to and centered on each optical element. Lenses L1 and L2 expanded the beam by a factor of 10. Once expanded, the beam was passed through an iris to remove aberrations at the beam edge. The expanded beam was then focussed down by the combination of lenses L3 and L4.

The beam diameter at the air–water interface was measured by mounting a razor blade on a precision stage which was located just above the water surface. For this measurement, the PSD was removed, allowing the beam to strike the ceiling of the laboratory, where it created a large, easily viewed spot. The blade was translated by the precision stage, and the locations where the blade just began to interrupt the laser beam, and where the beam was completely obscured were recorded. The difference between these two positions was 84 μm. In the experiments presented here, the smallest wavelength measured was $\lambda = 2.8$ mm, giving a worst-case wavelength-to-diameter ratio of 33, sufficient to resolve the wave slopes. The method used for measuring the beam diameter gives a value larger than the typically quoted $1/e^2$ diameter. Hence, the actual diameter is smaller, and the resolution better than that quoted here.

In the presence of waves, the air–water interface is deformed, and the laser beam is refracted due to the difference in the indices of refraction of air and water. A two-dimensional position sensitive detector (PSD) was mounted above the water surface to record the motion of the laser beam as it was refracted by the wave surface. The

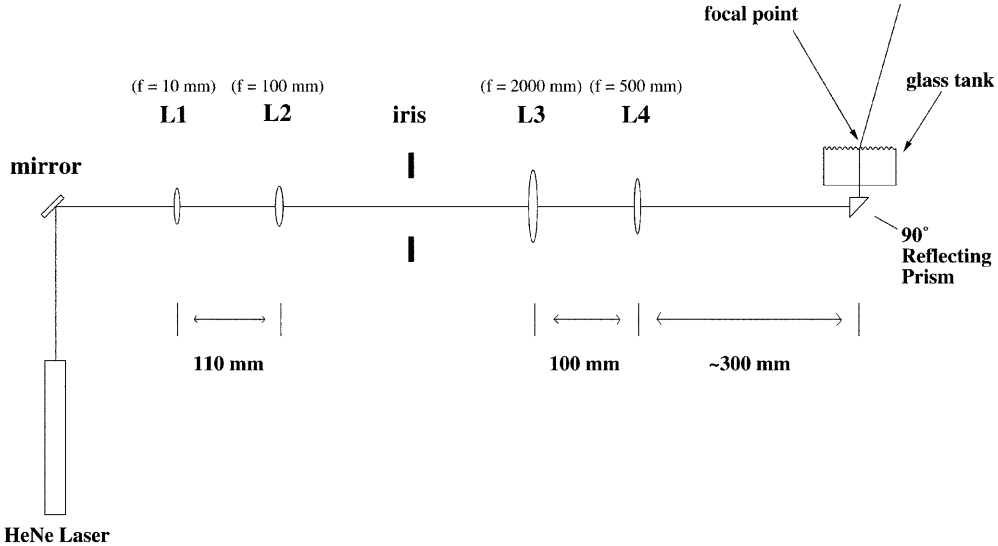

Fig. 4. Optics used for laser beam focusing. The optical train illustrated was placed between the laser and the 90° prism of Fig. 3

PSD was mounted on a precision three-dimensional stage, so its height above the water, as well as its position in a plane above the water could be accurately adjusted. The PSD outputs consist of an x and y voltage. Each voltage is linearly related to the location of the centroid of the light spot striking the sensor surface. An optical bandpass filter, centered on the HeNe wavelength was mounted in front of the PSD sensor so that light other than the laser beam was prevented from striking the sensor, thereby eliminating errors due to background room light. Knowledge of the location of the laser spot on the PSD surface, the distance of the PSD from the water surface, the indices of refraction of air and water, and Snell's law, permits computation of the wave slope.

For a perfect standing wave field, the slope at a fixed radial position varies periodically in time between a maximum and minimum value. Hence, at a given location in the tank, the laser beam oscillates back and forth, tracing a line on the surface of the PSD. The PSD was oriented so that this line was parallel to the y-axis of the sensor, resulting in a time-varying signal from the y output, and only a DC signal from the x output, simplifying the data reduction procedure.

Time traces from the PSD were recorded at 40–50 locations along the radius, depending on the particular experiment. The spatial separation between measurements was 95.25 μm. The laser beam was moved to each radial location by adjusting the horizontal position of the 90° prism, using the 3D translation stage upon which that prism was mounted. When the experiment was complete, the time-trace obtained at each radial location was processed to give the amplitude of the slope at that point. The wave slope envelope was obtained by plotting this amplitude against each of the radial locations where measurements were recorded.

3.2
Surfactant application

Experiments were conducted on water surfaces which were clean, as well as on water surfaces coated with a surfactant monolayer. Three different surfactants were employed: oleyl alcohol (white, Hormel Institute), stearic acid (Aldrich, 99+% purity) and hemicyanine (chemical name: 4-[4-(dimethylamino)styryl]-1-docosylpyridinium bromide; Aldrich). Experiments were conducted over a range of surface concentrations for each surfactant. Stock solutions of all surfactants were prepared in HPLC grade heptane. Care was taken to properly seal the container containing the stock solution to minimize evaporation of the heptane. Each container was also wrapped in paraffin film to further reduce any evaporative loss of heptane. Surfactant was deposited upon the water surface using a micrometer syringe in a drop-by-drop fashion. Upon deposition, the solution formed a liquid lens on the water surface, which left a surfactant monolayer behind as the heptane evaporated. The drops were applied slowly, so that each liquid lens completely evaporated before the next one was deposited. Upon completion of surfactant deposition, a 20-min waiting period was imposed to insure that the entire system was in equilibrium.

3.3
Cleaning procedure

Distilled water was used for all experiments. This water was obtained from a two stage distillation unit, fed by filtered tap water. The following cleaning procedure was employed before each experiment to insure cleanliness of the water in the circular wave tank. First, a peristaltic pump was used to remove water from the previous run by applying suction at the water surface so that surfactant monolayers were efficiently removed. The tank was then flushed with copious amounts of distilled water, overflowing the tank brim to eliminate residual surfactant monolayers. The suctioning process was then repeated. This process was performed a total of three times.

Following this cleaning procedure, the tank was filled to overflowing, creating a meniscus which bulged upward from the plane of the tank rim. The tank was filled to precisely the same level prior to each experiment, to eliminate any variations in the curvature of the meniscus at the tank edge. This was achieved by first creating a perfectly flat water surface, using the peristaltic pump to remove water until the meniscus was parallel to the tank rim. The point at which the meniscus was flat was ascertained by viewing one of the ceiling lights reflected on a region of the water surface very close to the tank rim. Viewing the light while slowly removing water from the tank, the point at which the meniscus became flat occurred when the image of the light was no longer distorted. Then, a known quantity of water was metered into the tank. Once the tank filling procedure was complete, experiments were initiated.

4
Results

A plot of the absolute value of the wave slope versus radial position is presented in Fig. 5 for two typical experiments conducted with stearic acid. Each point in Fig. 5 is the amplitude of a sinusoidal time trace obtained at that radial location. The two sets of data presented in this figure are for two different concentrations of stearic acid. The values for the radial location r in Fig. 5 are arbitrary. While it is known that the three peaks in the plots presented in this figure correspond to the fourth, fifth and sixth extrema in wave slope, the actual distance from the center of the tank was not measured. However, this value was obtained in the process of fitting the data to Eq. (11), as described in Sect. 2. This is illustrated in Fig. 6 where the data of Fig. 5 is replotted along with Eq. (11), and the x-axis corresponds to the correct radial location. The data in this figure, and for the rest of the experiments, were obtained along a radial segment, at locations approximately 6–10 mm from the tank center. As can be seen, the fit is quite good.

The goal of these measurements was to obtain values for α as a function of surfactant concentration c. As described in Sect. 2.4, both α and λ are obtained from the curve fitting procedure, so each of the experimentally obtained wave slope profiles obtained resulted in a single value of α and λ. Several experiments were conducted at each surfactant concentration, and the average values of α are presented in Fig. 7 for stearic acid, oleyl alcohol and

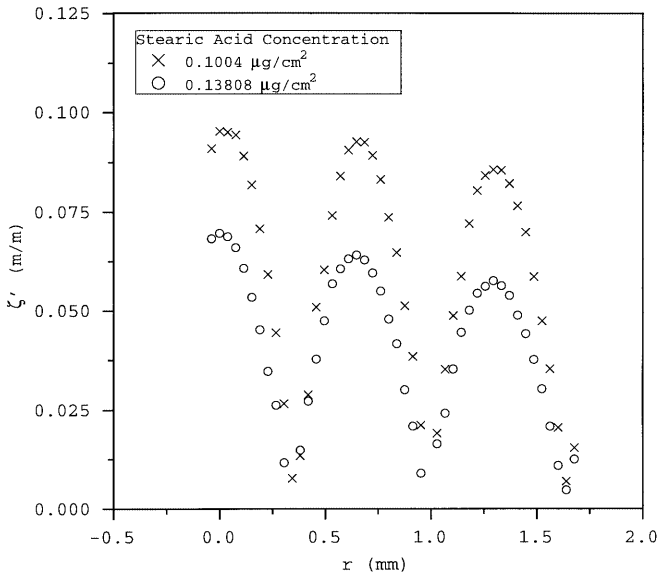

Fig. 5. Sample plot of the magnitude of the wave slope ζ' vs. radial position. Both sets of data are for stearic acid. The concentrations are: ×, 0.1004 μg/cm^2, ○, 0.1381 μg/cm^2

hemicyanine. The wavelength was not a strong function of the surface concentration, and that data is not presented here.

The form of the curve fits in Fig. 7a, b is

$$\alpha = \frac{D_1}{\sqrt{(c_0^{-2} - c^{-2})^2 + (D_2/c^2)}} \quad , \tag{13}$$

where D_1 and D_2 are constants which are tuned to best fit the data, and c_0 is the surface concentration where α is a maximum. The form of Eq. (13) is analogous to that for the amplitude response of a forced damped oscillator, an analogy first suggested by Bierwagen (1969) for wave damping by a surfactant monolayer. In this analogy, α corresponds to the amplitude response of the harmonic oscillator, and c corresponds to the oscillator frequency. The expected peak in the α versus c behavior was not observed for hemicyanine; a simple exponential curve fit is provided for the data in Fig. 7c.

Additional information which can be extracted from these measurements are the surface tension σ and surface elasticity E. These values can be obtained from the measured values of α and λ by use of the real and imaginary parts of the solvability condition for the coefficients A and B in Eqs. (7) and (8). The focus of this paper is the demonstration of an experimental method utilizing circular capillary waves and hence σ and E data are not presented here.

5 Discussion

Overall, the data obtained using the experimental method developed here is relatively noisy. In its current configuration, this method gives results whose scatter is comparable with, or slightly worse than recent measurements obtained using the method illustrated in Fig. 1. For example, Noskov and Zubkova (1995) obtained plots of α for

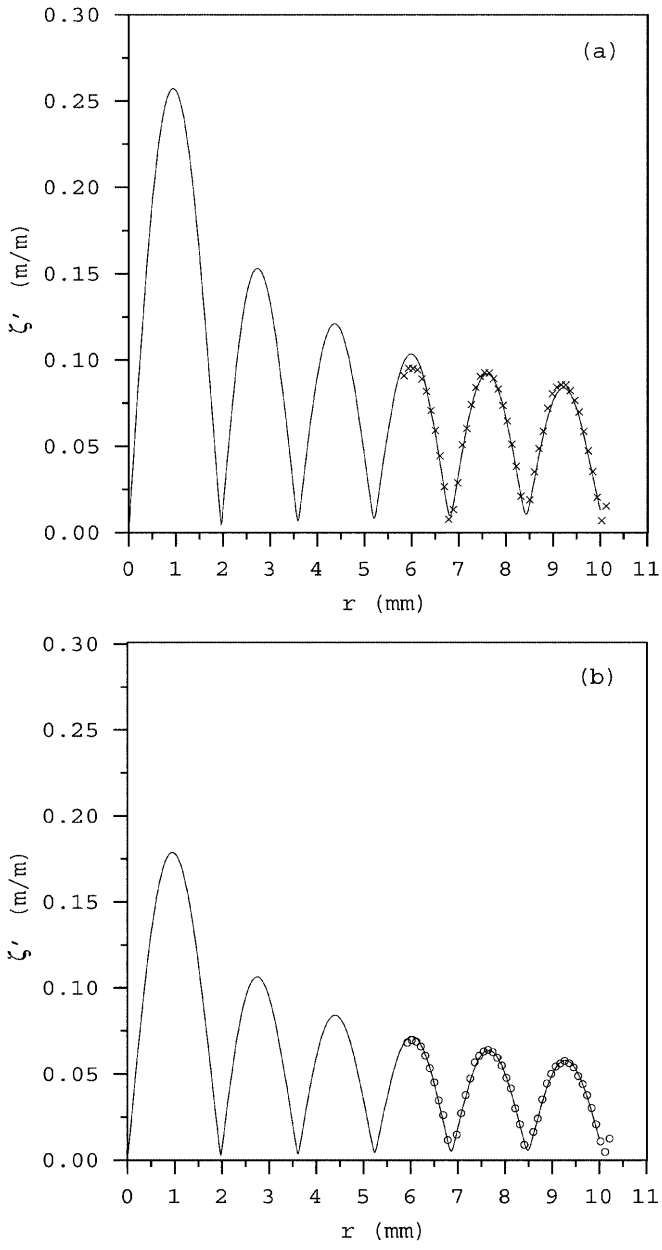

Fig. 6a, b. Plot of the data presented in Fig. 5, superimposed with Eq. (11). **a** c = 0.1004 μg/cm^2, **b** c = 0.1381 μg/cm^2

stearic acid showing a degree of scatter comparable to that presented in Fig. 7a. However, for a first implementation of this technique, these results are good.

Comparison of the decay coefficients obtained here with those obtained by other researchers is now presented. Stearic acid was investigated by Noskov (1988) on a 0.01 N hydrochloric acid substrate. Plots of α versus the surface concentration were presented at wave frequencies of 180 and 520 Hz, both of which reveal a peak in α at approximately 0.24 nm^2 mol^{-1}, which corresponds to c = 0.2 μg cm^{-2}, compared to the peak obtained here at c = 0.25 μg cm^{-2} for f = 120 Hz. Noskov and Zubkova (1995) present a plot of α versus surface concentration for stearic acid at f = 520 Hz showing a peak value for α located at c = 0.19 μg cm^{-2}. The maximum value was $\alpha \sim 1.9$ cm^{-1} compared to $\alpha \sim 0.5$ cm^{-1} in the current

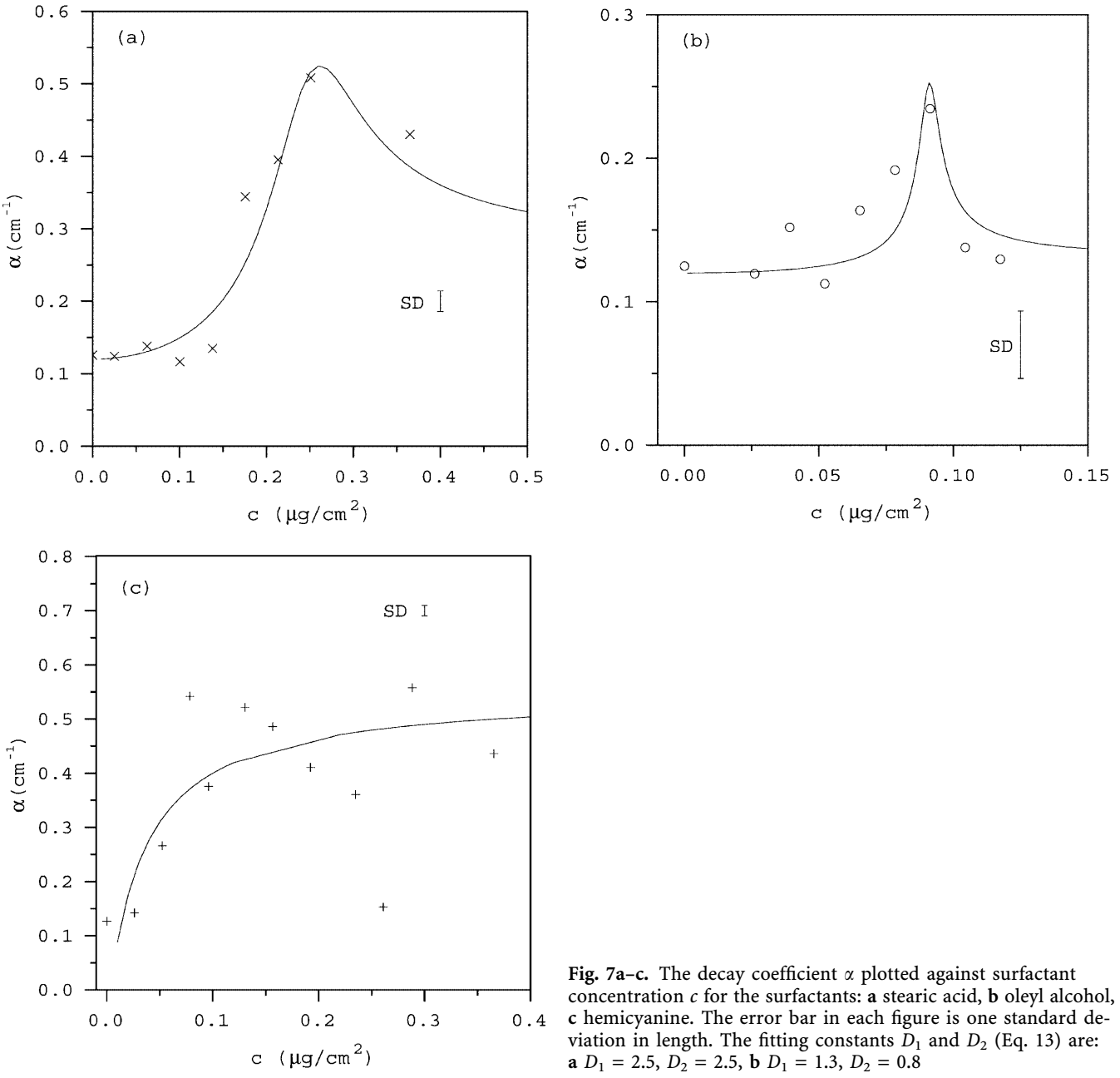

Fig. 7a–c. The decay coefficient α plotted against surfactant concentration c for the surfactants: **a** stearic acid, **b** oleyl alcohol, **c** hemicyanine. The error bar in each figure is one standard deviation in length. The fitting constants D_1 and D_2 (Eq. 13) are: **a** $D_1 = 2.5$, $D_2 = 2.5$, **b** $D_1 = 1.3$, $D_2 = 0.8$

work. The large difference between the values of α at the peak is expected, since α increases with wave frequency, and the frequency used in Noskov and Zubkova (1995) is over four times larger than in the present work.

Mass and Milgram (1998) obtained measurements of α for oleyl alcohol, over a range in wave frequencies $f = 4$–24 Hz, but do not provide values of α as a function of surface concentration. Barger (1991) provides data for α versus surface concentration for oleyl alcohol and reports a peak at a surface concentration of approximately $c = 0.05$ μg cm^{-2} at a frequency of 30 Hz, compared to the peak at $c = 0.09$ μg cm^{-2} at $f = 120$ Hz obtained here. Barger's peak value is $\alpha = 0.3$ cm^{-1}, which is actually slightly larger than the peak value of $\alpha = 0.24$ cm^{-1} obtained here. This is unexpected, since α is expected to increase with frequency. The reason for this discrepancy is unclear.

Other studies relevant to the surfactants presented here were not found in the literature. Values of α for hemicyanine were not found in the literature, and those presented here are believed to be the first reported.

There are several improvements to the technique presented here which would provide greater accuracy and reduced scatter. The first is the implementation of a lock-in amplifier. In a typical lock-in amplifier application (e.g., Hieftje 1972), a slowly varying signal modulates a higher frequency carrier signal of frequency f_c. The lock-in amplifier amplifies only portions of the signal within a bandwidth Δf of f_c and in phase with f_c. In the current application, the slope of a standing water wave is desired at several spatial locations. At each spatial location, a time trace is recorded whose frequency is that of the shaker vibration. The amplitude of this periodic time trace is the

quantity which is desired, since it is related to ζ'. If the frequency of the shaker vibration is considered to be f_c then the amplitude of the time trace can be extracted via lock-in amplification.

The signal-to-noise improvement ratio due to lock-in amplification is estimated as (Neelakantan et al. 1980)

$$\mathrm{SNIR} = \sqrt{\frac{f_c}{\Delta f}} \ , \tag{14}$$

where Δf is the bandwidth which is passed. The value of Δf is typically determined by the bandwidth of the signal which is modulating f_c. Here the signal which modulates f_c is the magnitude of the wave slope which should be a constant at any given point along the wave profile. Accordingly, Δf can be made arbitrarily small, the only practical limitation being that a reduction in Δf decreases the response time of the system, requiring longer waiting periods after moving to a new spatial location along the wave profile. Using a conservative value of $\Delta f = 0.1$ Hz and setting $f_c = 120$ Hz gives SNIR = 35, a significant improvement. Obviously even greater improvements can be obtained by reducing Δf.

Several other modifications to the experimental setup would be useful in reducing experimental scatter. The circular tank used was much deeper than necessary to insure that the waves generated were in the deep water regime. Convective cells caused by evaporation at the water surface may have resulted in some small disturbance of the wave field. Such convective cells can be damped by reducing the tank depth. Additionally, although the water used in these experiments typically sat in glass bottles overnight prior to use to insure that they were at room temperature, temperature variations in the overall apparatus may have existed, also contributing to measurement variations. Situating the entire apparatus in a thermostated environment would improve measurement scatter. Finally, automation of the traverse mechanism and data acquisition system would allow for a larger number of points along the waveform profile, improving the accuracy of α.

It is noted that in Fig. 7a, b, the α versus c data show a peak in damping coefficient at intermediate concentrations, an observation which has been made by many authors (e.g., Noskov and Zubkova 1995). The α data for hemicyanine does not display this behavior, however it is possible that the larger degree of scatter in this data set obscures this trend.

As illustrated in Fig. 6, data for wave slope was obtained over a radial segment of the wave field covering, roughly, the fourth, fifth, and sixth extremum in wave slope. This corresponds to the region of the third peak and trough in wave amplitude. We had hoped to obtain measurements even closer to the center of the tank, since the variation in wave slope is even greater at the center. However, the physical constraints of the tank assembly fixtures prevented us from obtaining data at the actual tank center. This may have actually been beneficial, since any imperfections in the tank roundness would have been focussed at the tank center, causing errors. Experiments which ascertain the optimal distance from the tank center, where the greatest accuracy and reproducibility exists, are needed.

6
Conclusion

Measurements of the decay coefficient α for a capillary wave field covered with monolayers of stearic acid, oleyl alcohol, and hemicyanine were reported. These measurements were conducted in a capillary wave facility having a circular geometry, which has rarely been used for the characterization of surfactant monolayers. The theory for these waves was developed for the first time avoiding the usual $|kr| \gg 1$ assumption. The results show a degree of scatter comparable to measurements obtained using the traditional rectangular capillary wave configuration. It is expected that simple improvements to the method would allow for much more accurate and reproducible results.

References

Allain C; Cloitre M (1988) Horizontal cylinders at a fluid interface: equilibrium, shape of the meniscus and capillary interaction. Ann Phys 13: 141–146

Barger WR (1991) A review of experimental observations and remaining questions concerning formation, persistence, and disappearance of sea slicks. NRL Report 9313 pp 1–46 Naval Research Laboratory, Washington, DC

Bendure RL; Hansen RS (1967) Capillary ripple investigations on monolayers at intermediate elasticities. J Phys Chem 71: 2889–2892

Bierwagen GP (1969) Comments on the shape of the damping coefficient curve for capillary waves, with an analogy to the amplitude response of a forced damped oscillator. J Colloid Interface Sci 31: 574–577

Edwards DA; Brenner H; Wasan DT (1991) Interfacial transport processes and rheology. Butterworth–Heinemann, Boston, Mass

Faraday M (1831) On the forms and states assumed by fluids in contact with vibrating elastic surfaces. Philos Trans Roy Soc London 121: 319–340

Garrett WD; Zisman WA (1970) Damping of capillary waves on water by monomolecular films of linear polyorganosiloxanes. J Phys Chem 74: 1796–1805

Hansen RS; Ahmad J (1971) Waves at interfaces. In: Progress in Surface and Membrane Science. Danielli JF; Rosenberg MD; Cadenhead DA eds, Vol. 4, pp 1–56. New York: Academic Press

Hansen RS; Lucassen J; Bendure RL; Bierwagen GP (1968) Propagation characteristics of interfacial ripples. J Colloid Interface Sci 26: 198–208

Hieftje GM (1972) Signal-to-noise enhancement through instrumental techniques: Part I. signals, noise, and S/N enhancement in the frequency domain. Anal Chem 44(6): 81A–88A

Hirsa A; Korenowski GM; Logory LM; Judd CD (1997a) Determination of surface viscosities by surfactant concentration and velocity field measurements for an insoluble monolayer. Langmuir 13: 3813–3822

Hirsa A; Korenowski GM; Logory LM; Judd CD (1997b) Velocity field and surfactant concentration measurement techniques for free-surface flows. Exp Fluids 22: 239–248

Jiang Q; Chiew YC; Valentini JE (1992) Damping of cylindrical propagating capillary waves on monolayer-covered surfaces. Langmuir 8: 2747–2752

Lucassen J; Hansen RS (1966) Damping of waves on monolayer–covered surfaces I. Systems with negligible surface dilational viscosity. J Colloid Interface Sci 22: 32–44

Mann JA; Ahmad J (1969) Dynamic surface tension: ripple damping. J Colloid Interface Sci 29: 158–161

Mann JA; Hansen RS (1963) Propagation characteristics of capillary ripples, II. Instrumentation for measurement of

ripple velocity and amplitude. J Colloid Interface Sci 18: 757–771

Mass JT; Milgram JH (1998) Dynamic behavior of natural sea surfactant films. J Geol Res 103: 15695–15715

Neelakantan K; Dattagupta S; Rajappan KP (1980) Signal to noise enhancement of lock-in amplifiers. Rev Sci Instrum 51: 251–252

Noskov BA (1988) Influence of a monolayer of stearic acid on damping of capillary waves. Kolloid Zh 50: 1201–1205

Noskov BA; Zubkova TU (1995) Dilational surface properties of insoluble monolayers. J Colloid Interface Sci 170: 1–7

Saylor JR; Handler RA (1997) Gas transport across an air/water interface populated with capillary waves. Phys Fluids 9: 2529–2541

Sohl CH; Miyano K; Ketterson JB (1978) Novel technique for dynamic surface tension and viscosity measurements at liquid–gas interfaces. Rev Sci Instrum 49: 1464–1469

Thiessen D; Scheludko A (1967) Dämpfung von zylindrischen stehenden Kapillarwellen durch grenzflächenaktive Stoffe. Kolloid-Z Z Polym 218(2): 139–148

Thiessen D; Schwartz A (1967) Stehende zylindrische Wellen an Flüssigkeitsoberflächen. Z Phys Chem 236: 363–368